Manufacturing and alignment tolerance analysis through Montecarlo approach for PLATO

Magrin, Demetrio, Ragazzoni, Roberto, Bergomi, Maria, Biondi, Federico, Chinellato, Simonetta, et al.

Demetrio Magrin, Roberto Ragazzoni, Maria Bergomi, Federico Biondi, Simonetta Chinellato, Marco Dima, Jacopo Farinato, Davide Greggio, Marco Gullieuszik, Luca Marafatto, Valentina Viotto, Matteo Munari, Isabella Pagano, Daniela Sicilia, Stefano Basso, Francesco Borsa, Mauro Ghigo, Daniele Spiga, Timothy Bandy, Mathias Brändli, Willy Benz, Giordano Bruno, Thierry De Roche, Daniele Piazza, Martin Rieder, Alexis Brandeker, Maximilian Klebor, Valery Mogulsky, Mario Schweitzer, Matthias Wieser, Anders Erikson, Heike Rauer, "Manufacturing and alignment tolerance analysis through Montecarlo approach for PLATO," Proc. SPIE 9904, Space Telescopes and Instrumentation 2016: Optical, Infrared, and Millimeter Wave, 99042Z (29 July 2016); doi: 10.1117/12.2232565

Event: SPIE Astronomical Telescopes + Instrumentation, 2016, Edinburgh, United Kingdom

Manufacturing and alignment tolerance analysis through Montecarlo approach for PLATO

Demetrio Magrin*[a], Roberto Ragazzoni[a], Maria Bergomi[a], Federico Biondi[a], Simonetta Chinellato[a], Marco Dima[a], Jacopo Farinato[a], Davide Greggio[a,b], Marco Gullieuszik[a], Luca Marafatto[a], Valentina Viotto[a], Matteo Munari[c], Isabella Pagano[c], Daniela Sicilia[c], Stefano Basso[d], Francesco Borsa[d], Mauro Ghigo[d], Daniele Spiga[d], Timothy Bandy[e], Mathias Brändli[e], Willy Benz[e], Giordano Bruno[e], Thierry De Roche[e], Daniele Piazza[e], Martin Rieder[e], Alexis Brandeker[f], Maximilian Klebor[g], Valery Mogulsky[g], Mario Schweitzer[g], Matthias Wieser[g], Anders Erikson[h], Heike Rauer[h]

[a]INAF – Osservatorio Astronomico di Padova, Vicolo dell'Osservatorio 5, 35122 Padova, Italy

[b]Dipartimento di Fisica ed Astronomia – Università degli Studi di Padova, Vicolo dell'Osservatorio 3, 35122 Padova, Italy

[c]INAF – Osservatorio Astrofisico di Catania, Via S.Sofia 78, 95123 Catania, Italy

[d]INAF – Osservatorio Astronomico di Brera, Via Brera 28, 20121 Milano, Italy

[e]Physics Institute, Space Research & Planetary Sciences, University of Bern, Sidlerstr. 5, CH-3012 Bern, Switzerland

[f]Department of Astronomy – Stockholm University, SE-106 91 Stockholm, Sweden

[g]OHB System, Manfred-Fuchs-Straße 1, 82234 Weßling – Oberpfaffenhofen, Germany

[h]DLR – Institut für Planetenforschung, Rutherfordstraße 2, 12489 Berlin, Germany

ABSTRACT

The project PLAnetary Transits and Oscillations of stars (PLATO) is one of the selected medium class (M class) missions in the framework of the ESA Cosmic Vision 2015-2025 program. The main scientific goal of PLATO is the discovery and study of extrasolar planetary systems by means of planetary transits detection.

According to the current baseline, the scientific payload consists of 34 all refractive telescopes having small aperture (120mm) and wide field of view (diameter greater than 37 degrees) observing over 0.5-1 micron wavelength band. The telescopes are mounted on a common optical bench and are divided in four families of eight telescopes with an overlapping line-of-sight in order to maximize the science return. Remaining two telescopes will be dedicated to support on-board star-tracking system and will be specialized on two different photometric bands for science purposes.

The performance requirement, adopted as merit function during the analysis, is specified as 90% enclosed energy contained in a square having size 2 pixels over the whole field of view with a depth of focus of +/-20 micron. Given the complexity of the system, we have followed a Montecarlo analysis approach for manufacturing and alignment tolerances. We will describe here the tolerance method and the preliminary results, speculating on the assumed risks and expected performances.

Keywords: Space telescope, wide field camera, tolerance analysis, extra-solar planetary system, asteroseismology.

1. INTRODUCTION

The project PLAnetary Transits and Oscillations of stars (PLATO) is the medium size mission (M3) selected by the European Space Agency (ESA) in the framework of the Cosmic Vision 2015-2025 program. The main scientific goal [1] of PLATO is to discover and characterize a large number of extrasolar planetary systems, providing the first catalogue of potentially habitable planets with known mean densities and ages. The exoplanet mean densities will be retrieved by coupling the information of the planet radius provided by PLATO via photometric transit method with the information of the planet mass obtained through radial velocity measurements of dedicated ground-based telescopes follow-up. Stellar masses, radii and ages are derived by asteroseismic analyses of the photometric light curves.

*demetrio.magrin@oapd.inaf.it; phone +39 049 8293540

Space Telescopes and Instrumentation 2016: Optical, Infrared, and Millimeter Wave, edited by Howard A. MacEwen, Giovanni G. Fazio, Makenzie Lystrup, Proc. of SPIE Vol. 9904, 99042Z · © 2016 SPIE · CCC code: 0277-786X/16/$18 · doi: 10.1117/12.2232565

The scientific payload [2], accordingly to the baseline presented to the ESA System Requirement Review (SRR), consists of 34 cameras mounted on a common optical bench. Two cameras, namely fast cameras, are dedicated to improve the pointing stability performance of the spacecraft on-board star-tracking system and will be specialized in two different photometric bands (blue 500-675 nm, red 675-1000 nm) for science purposes. The remaining 32 cameras, namely normal cameras, will observe in panchromatic mode between 500 and 1000 nm. They are divided in four groups of 8 cameras each. Each camera of a group will share the same line of sight and provides a sky area of about 1037 degrees^2, while the four groups point towards a sky direction which is displaced by about 9.2 degrees from the center of the overall field of view. This configuration allows the increasing of the overall instantaneous coverage to about 2124 degrees^2, with overlapping portions of sky covered by multiple groups, maximizing the science return. A scheme of the overlapping line of sight is shown in Figure 1. A detailed mission overview is given in [3].

Each camera is basically composed of a telescope optical unit (TOU), i.e. the optical components and the mechanical structure, a focal plane module (FPM), a front-end electronic (FEE) and camera support structure (CSS). For the aim of this work we will focus on the TOU, and in particular on the analysis of the optical manufacturing and alignment tolerances.

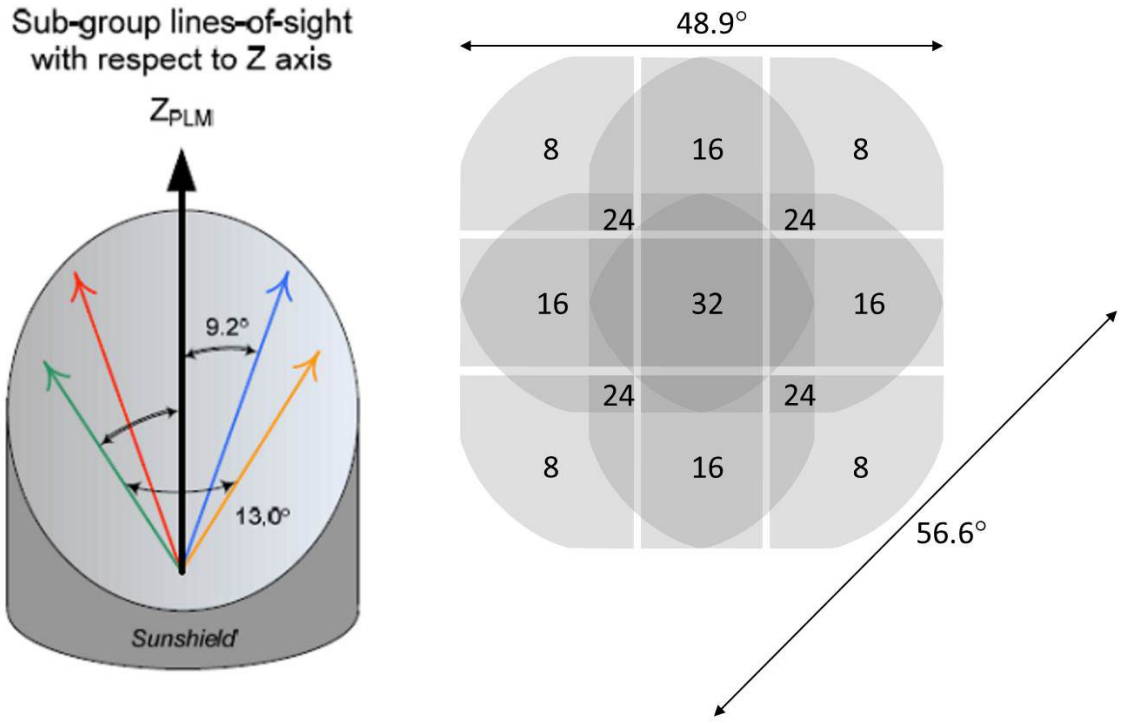

Figure 1. The overlapping line-of-sight concept (left) and the resulting field-of-view configuration (right).

2. TOU OPTICAL CONFIGURATION

The TOU optical configuration has been modified with respect to the baseline of the pre-selection phase [4], following the refinement and the maturity of the requirements. The optical configuration reported in the following refers to the baseline presented to the ESA SRR.

All the TOUs, 32 N-TOUs and 2 F-TOUs, have the same optical design but for the filter selecting the proper wavelength band. The TOU optical configuration consists of a window, placed at the entrance of the telescope, six lenses, and a physical aperture representing the stop of the optical system. The TOU focuses incoming collimated beams onto a focal plane, on which the FPA is positioned. A layout of the design is shown in Figure 2, while optical elements parameters, referring to nominal working temperature (-80°C) and pressure (0 atm), are reported in Table 1.

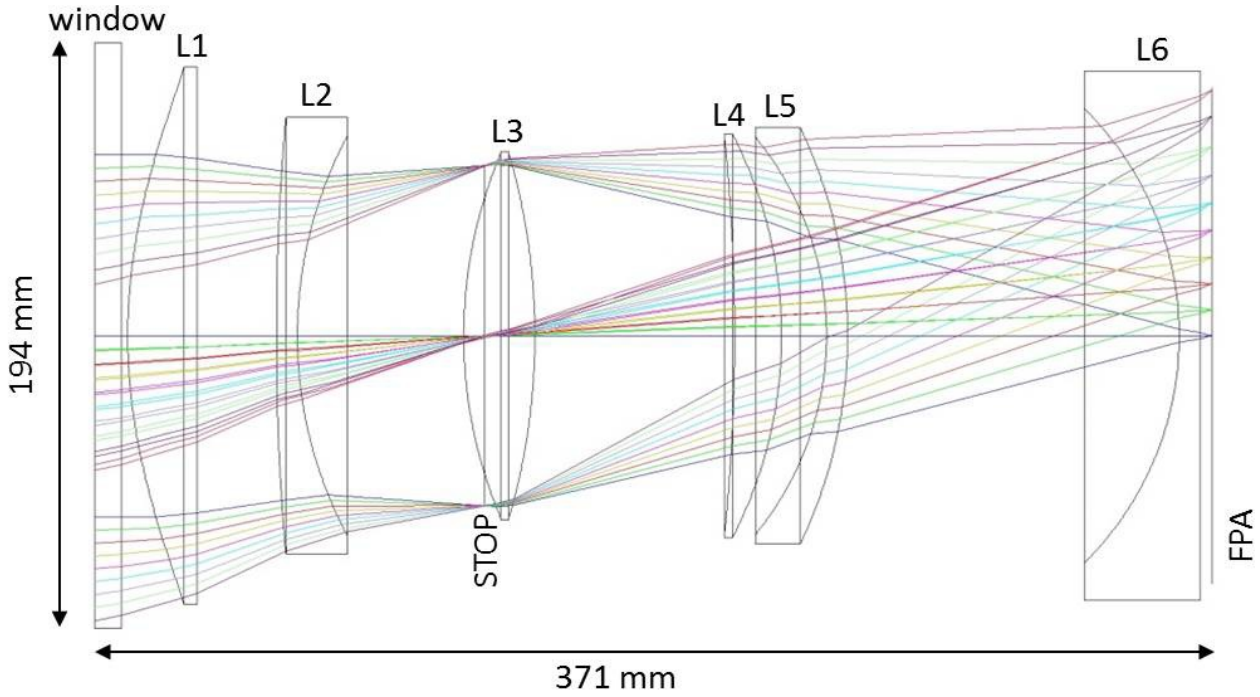

Figure 2. TOU optical layout.

Table 1. Optical elements parameters of the baseline in working conditions.

Label Optical Element		Radius of Cuvature (*) [mm]	Thickness [mm]	Aspheric Terms K	a^4	a^6	Glass	Aperture Shape	Clear aperture Diameter/Size [mm]	Physical aperture Diameter/Size [mm]	Physical Edge Thickness [mm]
Window	Surf. 1	-	9.000	-	-	-	SUPRASIL	Circular	190.000	194.000	9.000
	Surf. 2	-	2.000	-	-	-			190.000	194.000	
L1	Surf. 1	183.457	23.000	-3.87445	3.1477E-08	-4.0894E-12	S-FPL51	Circular	174.000	178.000	4.242
	Surf. 2	-	26.328	-	-	-			174.000	178.000	
L2	Surf. 1	824.888	7.000	-	-	-	N-KZFS11	Circular	140.800	144.800	20.420
	Surf. 2	140.673	62.198	-	-	-			128.260	132.260	
STOP		-	-7.000	-	-	-	-	Circular	112.608	112.608	-
L3	Surf. 1	154.050	23.600	-	-	-	LITHOTEC CAF2	Circular	116.600	120.600	2.612
	Surf. 2	-217.608	66.313	-	-	-			117.800	121.800	
L4	Surf. 1	-648.079	15.600	-	-	-	S-FPL51	Circular	129.400	133.400	2.739
	Surf. 2	-145.416	14.909	-	-	-			129.800	133.800	
L5	Surf. 1	-103.623	7.000	-	-	-	S-FTM16	Circular	128.000	132.000	15.016
	Surf. 2	-159.281	110.051	-	-	-			134.000	138.000	
L6	Surf. 1	-105.733	7.000	-	-	-	N-BK7 (G18)	Circular (**)	146.600 (**)	150.600 (**)	38.508 (**)
	Surf. 2	-	4.000	-	-	-			171.400 (**)	175.400 (**)	
FPA		-	-	-	-	-	-	Square	164.776	164.776	-

(*) Positive radius of curvature means convex surface, negative radius of curvature means concave surface.
(**) L6 has a particular shape (see description in the text). It will be cut in such a way to exploit only the FoV covered by FPA minimizing the lens mass. In the table, it is reported data related to the circular shape which envelope contains L6.

The insertion of the window as first optical element is due to multiple purposes: it allows to mitigate the thermal shock on the first lens during the launch; it shields the first lens (glass SFPL51, moderate rad-hardened glass) from direct incoming high energy radiation (mainly solar protons) and, for this purpose, the current window material is SUPRASIL; for N-TOUs the window allows to deposit in its internal surface a high-pass filter with cutoff wavelength at 500 nm able to define the blue edge of the wavelength spectral range. The red edge is determined by the detector quantum efficiency. For the two F-TOUs, the filter on the window second surface is a pass-band filter allowing the selection of spectral range 500-675 nm for the blue F-TOU and 675-1000 nm for the red F-TOU. The first surface of the front lens presents even aspheric terms (K, a^4, a^6), while the second surface has been imposed to be flat in order to facilitate the surface

interferometric measurement during lens manufacturing. The aspheric terms have been introduced to increase the FOV matching the quality requirements.

The stop of the optical system is a physical circular aperture located in front of the third lens. The stop diameter has been set to about 112.608 mm in order to deliver a real entrance pupil diameter of 120 mm. All the other lenses (L2, L3, L4, L5 and L6) present standard spherical surfaces.

The clear apertures of the lenses have been defined through a trade off with optical elements overall mass. In particular, in order to reduce the impact on the mass, the lenses clear apertures have been undersized, introducing as consequence mechanical vignetting. The amount of mechanical vignetting at the edge of the FoV (field having coordinates 13.6, 13.6 degrees, i.e. radial distance from the line of sight 18.876 degrees) has been estimated to be about 3.6%. In the optical model, this effect has been introduced by downsizing the entrance window aperture and then we have set the other lenses clear aperture diameters paying attention to not introduce further vignetting.

The last lens, the one in front of the FPA, will be cut in such a way to exploit only the FoV covered by FPA (avoiding further vignetting) in order to reduce its weight. A scheme representing L6 shape and a 3D view of the TOU structure are shown in Figure 2. In the radiation analysis results, the expected radiation dose for L6 will deteriorate excessively its transmissivity. For this reason, the L6 glass has been set to radiation hardened version of N-BK7, i.e. N-BK7 grade 18.

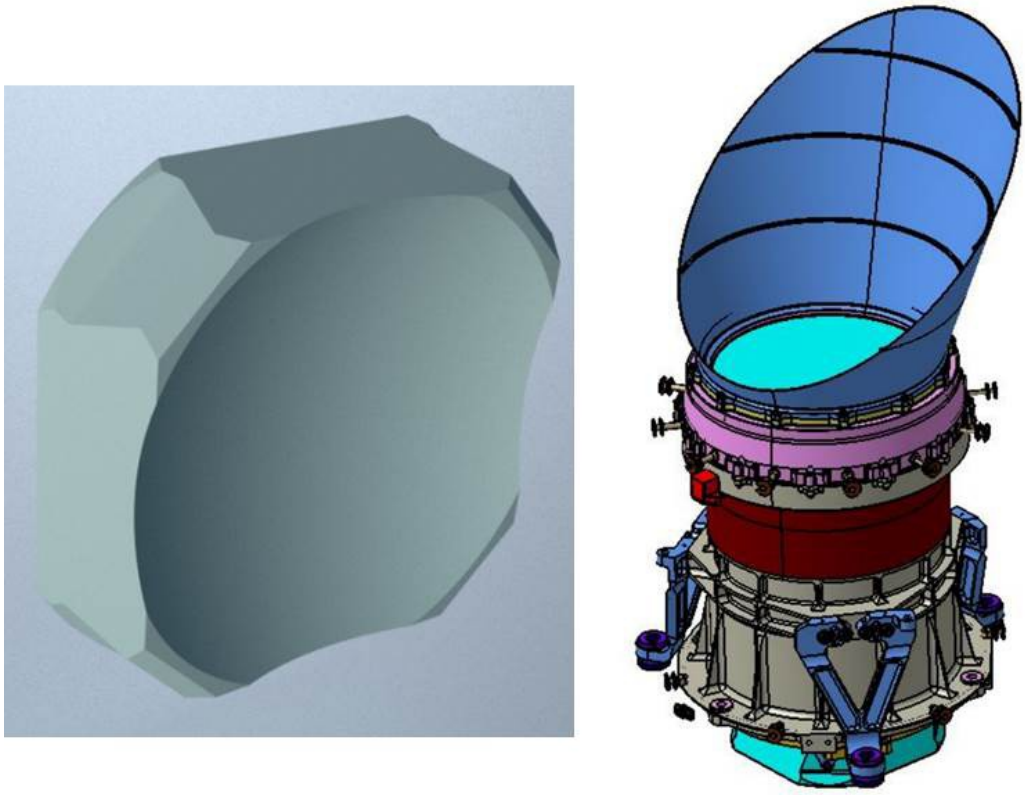

Figure 3. L6 shape (left) and TOU structure (right).

During the optimization process we have considered as optical system performance goal criteria the 90% polychromatic geometrical enclosed energy in 2×2 pixels^2 with respect to centroid at nominal working temperature (-80°C) and pressure (0 atm) and a depth of focus of ± 20 μm on the FPA. The weight assigned to the wavelengths has been derived by taking into account the foreseen detector quantum efficiency and the G0 star spectrum. The polychromatic (500-1000nm) enclosed energy as function of the focal plane position has been evaluated for the fields (0.0, 0.0) degrees, (0.0, 2.0) degrees, (0.0, 4.0) degrees, (0.0, 6.0) degrees, (0.0, 8.0) degrees, (0.0, 10.0) degrees, (0.0, 12.0) degrees, (0.0, 14.0) degrees, (0.0, 16.0) degrees, (0.0, 17.7) degrees, (13.6, 13.6) degrees. A scheme of the considered fields on the FPA surface and the enclosed energy as function of the focal plane position are shown in Figure 4.

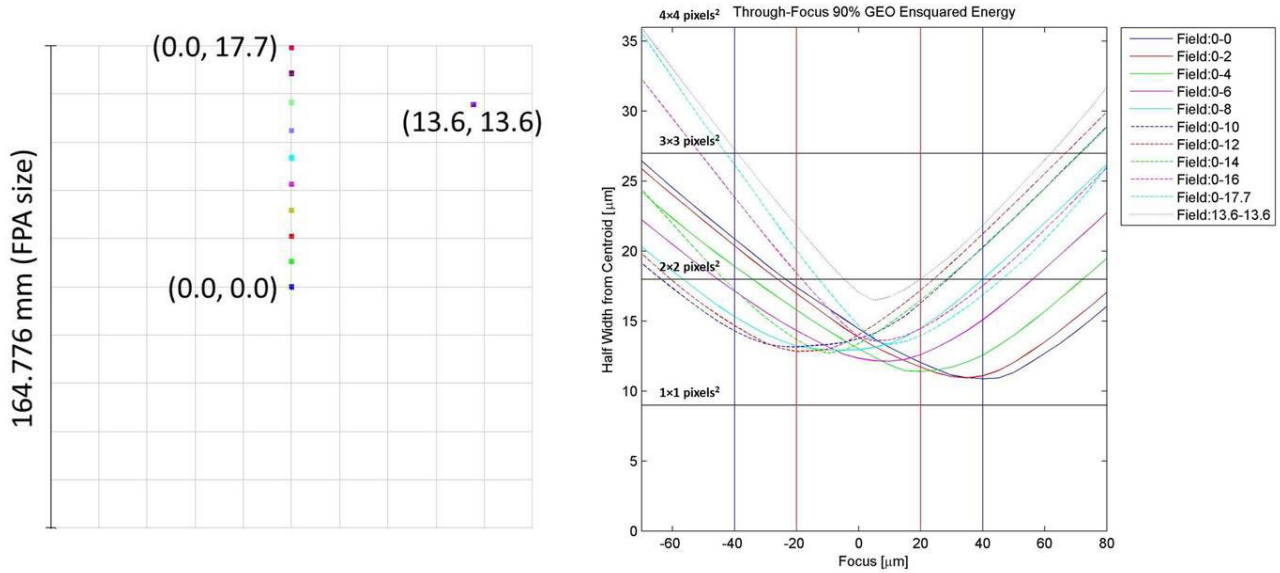

Figure 4. Fields position on the FPA (left) and 90% polychromatic geometrical enclosed energy as function of the focal plane position (right).

The performance is matched on the nominal focal plane position over the whole nominal FoV, while PSFs size is marginally out of specification in the depth of focus range. In particular at the very edge of the depth of focus range the performance is maintained within a circular FoV having radius equal to about 16 degrees (instead of 18.8875 degrees).

3. MANUFACTURING AND ALIGNMENT TOLERANCE PROCESS

We have performed a preliminary tolerance analysis on the optical configuration described in the previous section in order to individuate the optical system worst offenders and determine the order of magnitude of the tolerated errors. Given the aim of this analysis, we have considered the optical design in the nominal working temperature (-80°C) and pressure (0 atm), it is expected in fact that differences with respect to the room environment will be of the same order of accuracy. For this analysis, we have considered 10 reference fields (a scheme is shown in Figure 5). The fields are arranged along three different radial directions having relative angle of 120 degrees. While the nominal performances have been computed for the nominal design that presents rotational symmetry, this is no longer the case for the tolerance model. Excluding the central field, each radial direction is composed by three fields having radial distance 6.0 degrees, 12.0 degrees and 18.8 degrees respectively.

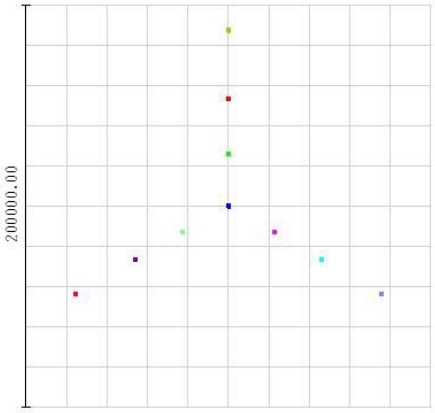

Figure 5. Scheme of reference fields considered during the tolerance analysis process.

As merit function we have considered the RMS spot radius of the reference fields. Then the performance in terms of polychromatic geometrical enclosed energy has been verified a posteriori.

The optical model for tolerances analysis has been implemented as follows. For each optical element, surfaces curvature radius (or flatness), surface irregularity, refractive index, Abbe number, central thickness and wedge are varied within the manufacturing maximum change that has been set in the model after an iterating process.

For what concerns the refractive indexes and Abbe numbers, we required to measure them with precision ±3×10-5 and ±2×10-5 respectively corresponding to both SCHOTT and OHARA standard certificate. The surfaces irregularity has been represented with half spherical aberration, and half astigmatism (random direction). In the case of L1 aspherical surface, irregularity and aspherical shape error has been simulated by superimposing an error of 50 nm RMS to the original surface, with spatial frequency determined by Zernike polynomials from 4 to 37 (each polynomial has the same weight).

We have assumed that, during the alignment process, the wedge of the lenses can be compensated so that the two local normal vectors to the two surfaces of the lens at the center make the same angle with the nominal telescope optical axis. In this way we are mimicking the tilt alignment process based on back reflected Newton rings. An error is then added to the lens tilt representing the required precision of the tilt alignment process. The error on the lenses position has been simulated as absolute position error of the first surface of each optical element, so that we have not introduce any compensation based on the relative position between the optical elements. In the current alignment process, lenses relative distances will be maintained under control with a method based on Hartmann mask, so that we expect that the precision in defocus position will be even better.

As further compensators, we have assumed the relative distance between L6 last surface and the FPA plane and the two tilt angles of the FPA (FPA has been assumed to be centered with respect to the chief ray of the field having coordinates (0.0, 0.0) degrees).

The orders of magnitude of the maximum change for the considered offenders are reported in Table 2.

Table 2. Manufacturing and alignment offenders maximum changes.

Offenders	Type	Maximum change
Refractive index	Manufacturing	$\pm 3\times10^{-4}$
Abbe Number	Manufacturing	±0.2÷0.3%
Central Thickness	Manufacturing	±0.10÷0.02 mm
Wedge	Manufacturing	±1.4÷0.7 arcmin
Curvature Radius	Manufacturing	±0.40÷0.02 mm
Surface Flatness	Manufacturing	±0.5 fringes
Surface Irregularity	Manufacturing	±1.0÷0.3 fringes
Tilt	Alignment	±2.4÷0.7 arcmin
Decenter	Alignment	±0.04÷0.02 mm
Defocus	Alignment	±0.04÷0.02 mm

4. TOLERANCE ANALYSIS RESULTS

Performances have been estimated by mean of a statistical approach: we have simulated a distribution of 5000 Montecarlo realizations. The histogram representing the Montecarlo distribution as function of the RMS spot radius Merit Function is shown in Figure 6. In the histogram, we have over-plotted the Merit Function values representing the nominal case, the 50 percentile, 90 percentile, the 98 percentile and the worst case and we have indicated the corresponding size of the box enclosing the 90% of the energy for the worst field in a typical representative realization.

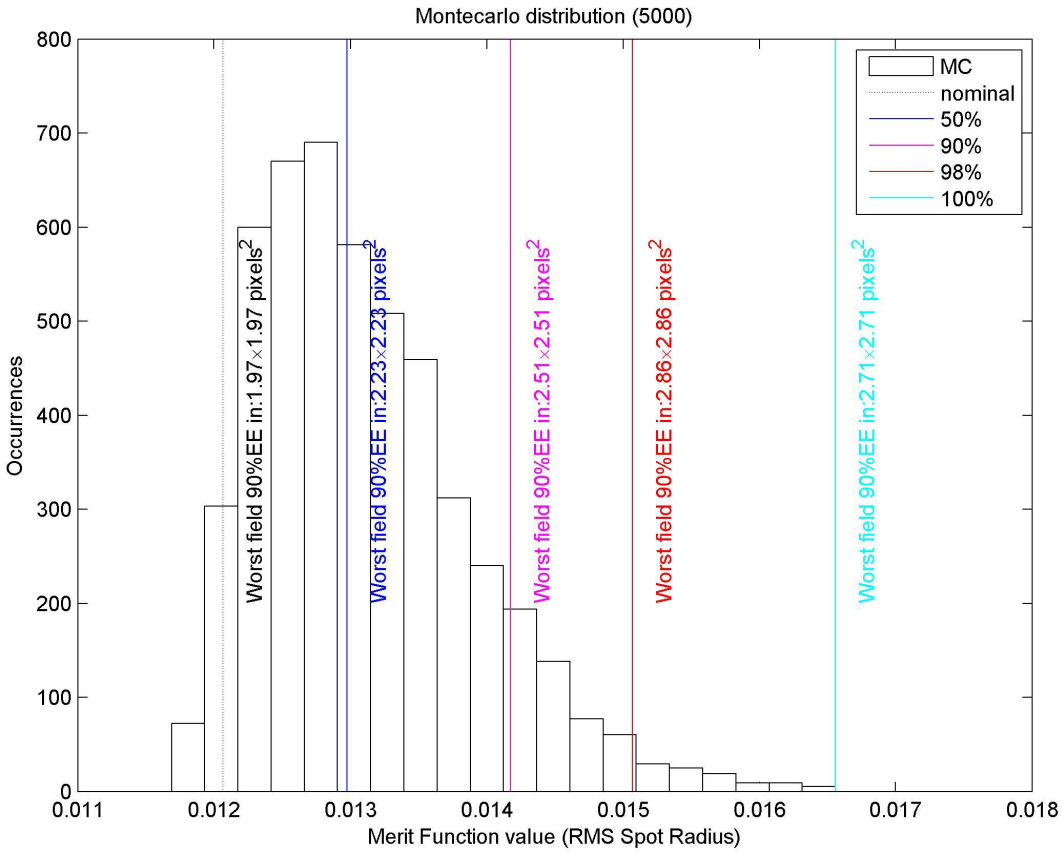

Figure 6. Tolerance Montecarlo distribution (5000 realizations) as function of the Merit Function (RMS spot radius). The nominal case, the 50 percentile, 90 percentile, the 98 percentile and the worst case are over-plotted with different colored lines. For each case, the 90% geometrical enclosed energy size for the worst field of one representative realization is highlighted.

It has to be noticed that the obtained distribution of the 5000 realizations assumes full uncorrelation among the various discrepancies in the alignment and in the manufacturing. In reality this will be not, strictly speaking, true. The overall number of planned TOUs flight models will be 37 (32 N-TOUs, 2 F-TOUs and 3 spares) and the number of optical components will be likely even slightly larger than this figure. This means that once all the parameters (curvature radii, thicknesses, wedges, etc.) are known, they can be combined in an optimized manner. Furthermore, even during the alignment procedure, as the measurement of misalignment is often more accurate than the positioning ability itself, it can happen that in some cases some TOUs will be partly aligned within a certain accuracy, so that proper and special efforts can be dedicated to the one deserving it, so skewing the distribution curve artificially toward a best performance. All this speculation has not been considered during the following calculation.

The projection of the Montecarlo distribution onto the actually foreseen 37 TOUs, translates into the condition that, with a high degree of statistical confidence, the worst of the whole set of TOUs will correspond to the quality identified by the 36/37 percentile (about 97.3%) and that, assuming no spare is going to be used, the TOUs flight models should exhibits a quality corresponding to 34/37 percentile (about 91.9%). In the following, the 90 and 98 percentile worst samples should be intended to illustrate the expected worst quality of the TOU ensemble with the modelled distribution of manufacturing and alignment errors.

In order to have a general view of the performance figure, we have computed the geometrical enclosed energy as function of the FPA position for a representative realization corresponding to the 50 percentile, 90 percentile, the 98 percentile and the worst case. The plots are shown in Figure 7.

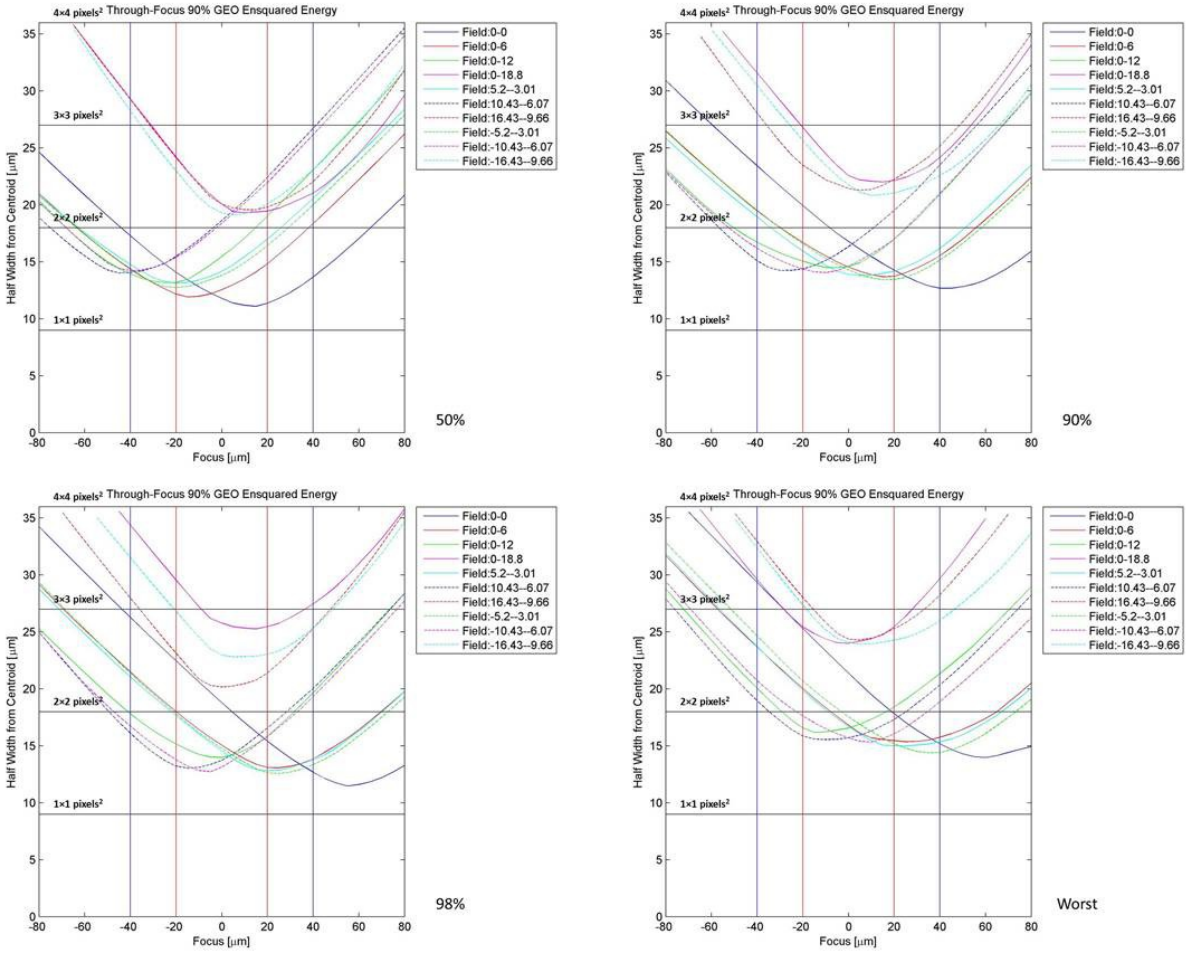

Figure 7. Polychromatic geometrical enclosed energy as function of the FPA position for a representative realization of the 50 percentile (top-left), 90 percentile (top-right), the 98 percentile (bottom-left) and the worst case (bottom-right).

Once tolerance process is introduced from a distribution of a large number of randomly variable sources of errors in manufacturing and alignment, any simple symmetry distribution of the optical quality on the focal plane is lost, and, as consequence, it is difficult to associate a single merit function for each possible realization. As requirements often point to the worst optical quality over the whole FoV, the issue of how the quality is distributed over the FoV unavoidably folds out. The same worst quality could be marginally obtained, in fact, on a small area on the FoV edge, or consistently over a significant portion of it, making the science capabilities affected in very different manners. Average of any kind also consistently suffers of a similar issue.

However, the production of detailed map is time consuming (each of the following maps requires about 31 hours of computing time on a 28 CPUs machine) and, to a certain extent, are just representative of examples that are produced synthetically. Here, we present a few of them in order to exhibit typical behaviors of 98 percentile worst samples.

Each map has been generated by computing the polychromatic geometrical enclosed energy for each field having sky coordinates X and Y in the range from -18.0 degrees to +18.0 degrees with step of 1.0 degrees in both directions. The following percentages of sky area have been computed by applying a bi-linear interpolation to the previous map with step of 0.05 degrees.

We have analyzed the behavior of a 98 percentile typical realization. The contour plots highlighting the percentage of polychromatic geometrical enclosed energy contained in 2×2 pixels^2 and the size of the square box (in pixels) containing the 90% of polychromatic geometrical enclosed energy, for a focal plane defocus equal to -0.020 mm, the nominal focal plane position and a focal plane defocus equal to +0.020 mm are shown in Figure 8.

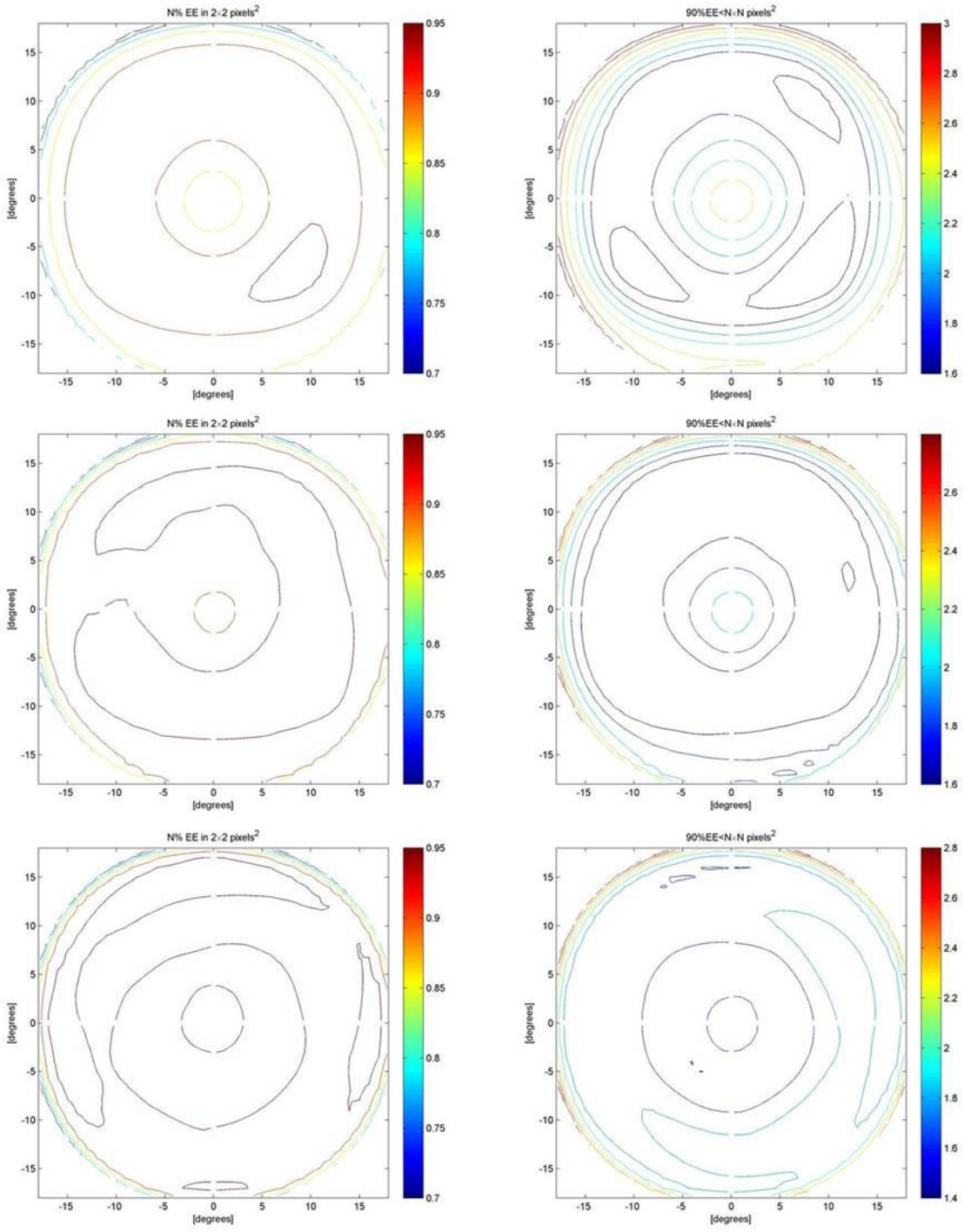

Figure 8. Percentage of polychromatic geometrical enclosed energy contained in 2×2 pixels^2 (left column) and size of the square box in pixels containing the 90% of polychromatic geometrical enclosed energy (right column). From top to bottom, the maps refer to defocused focal plane by -0.020 mm, nominal focal position and defocused focal plane by +0.020 mm. Maps refer to a 98 percentile typical realization.

Given the maps, one can compute the percentage of sky area (normalized to the nominal one) into which a given percentage of polychromatic geometrical enclosed energy is contained in 2×2 pixels2, or into which the 90% of polychromatic geometrical enclosed energy is contained in a given square box size. Results of this computation are shown in Table 3 and Table 4 respectively.

Table 3. Percentage of sky area (normalized to the nominal one) into which a given percentage of polychromatic geometrical enclosed energy is contained in 2×2 pixels^2 (98 percentile realization).

		Percentage of Sky Area [%]		
	%EE	FPA defocus		
	[%]	-0.020 mm	0 mm	+0.020 mm
N%EE≤2×2 pixels^2	70	99.94	99.99	99.98
	75	99.40	99.79	99.64
	80	97.71	99.02	98.62
	85	88.40	97.15	96.59
	90	59.48	90.29	92.94
	95	3.31	40.91	39.28

Table 4. Percentage of sky area (normalized to the nominal one) into which the 90% of polychromatic geometrical enclosed energy is contained in a given square box size (98 percentile realization).

		Percentage of Sky Area [%]		
	N	FPA defocus		
	[pixel]	-0.020 mm	0 mm	+0.020 mm
90%EE≤N×N pixels^2	1.6	10.42	53.79	20.09
	1.8	44.01	75.99	68.12
	2.0	59.52	90.68	93.18
	2.2	72.01	96.11	96.47
	2.4	86.34	98.43	98.51
	2.6	94.23	99.52	99.60
	2.8	97.84	99.93	99.94
	3.0	99.47	99.99	99.99

Summarizing the results: even considering the worst 98 percentile of a random distribution, roughly corresponding to the worst TOU of the produced ensemble (32 N-TOUs, 2 F-TOUs and 3 spares), and the whole depth of focus (±20 μm), more than 90% of the nominal FoV is characterized by having a PSF whose 90% polychromatic geometrical enclosed energy is contained in a square box with size less than 2.6 pixels. In most of the other cases, the vast majority of the Field of View stays well within 2.2×2.2 pixels^2.

It is evident from an inspection of the distribution of the 90% polychromatic geometrical enclosed energy as function of the focal plane defocus (Figure 7 and Table 4) that for the 98 worst percentiles the median of the region where the defocus still gives acceptable performances is skewed (negative defocus gives worst result than the positive one). Once such a TOU is characterized, one could use this to redefine the nominal focal position to lie symmetrically. While this approach potentiality further increases the robustness of the optical design, it has not been yet implemented in this analysis but it has to be considered as a further element of margin in the tolerance analysis.

5. CONCLUSIONS

The nominal optical configuration of the TOU (ESA SRR) for the PLATO mission has been illustrated together with the expected performances in terms of 90% polychromatic geometrical enclosed energy within a depth of focus of +/-20 micron. We have presented the assumptions on the manufacturing and alignment tolerances implemented in the analysis. Given the difficulty to operatively check the performance requirement with standard method, we have followed a statistical approach, speculating on the number of TOUs to be realized and on the percentage of sky area delivering a certain performance. As net result, we have obtained that, even considering the 98 percentile of a Montecarlo distribution of 5000 realizations (corresponding statistically to about 1 TOU out of spec over 37 manufactured TOUs), the 90% polychromatic geometrical enclosed energy within a depth of focus is upper bounded by 2.6×2.6 pixels^2 (while in the vast majority Field of View it stays well within 2.2×2.2 pixels^2). This value has to be intended as an upper limit, given the fact that no attempt to consider FPA alignment optimization has been carried out during the analysis.

6. ACKNOWLEDGMENTS

This study was supported by the Italian Space Agency (ASI) – Contract number 2015-019-R0.

REFERENCES

[1] Rauer, H.; Catala, C.; Aerts, C.; Appourchaux, T.; Benz, W.; Brandeker, A.; Christensen-Dalsgaard, J.; Deleuil, M.; Gizon, L.; Goupil, M.-J.; Güdel, M.; Janot-Pacheco, E.; Mas-Hesse, M.; Pagano, I.; Piotto, G.; Pollacco, D.; Santos, Ċ.; Smith, A.; Suárez, J.-C.; Szabó, R.; Udry, S.; Adibekyan, V.; Alibert, Y.; Almenara, J.-M.; Amaro-Seoane, P.; Eiff, M. Ammler-von; Asplund, M.; Antonello, E.; Barnes, S.; Baudin, F.; Belkacem, K.; Bergemann, M.; Bihain, G.; Birch, A. C.; Bonfils, X.; Boisse, I.; Bonomo, A. S.; Borsa, F.; Brandão, I. M.; Brocato, E.; Brun, S.; Burleigh, M.; Burston, R.; Cabrera, J.; Cassisi, S.; Chaplin, W.; Charpinet, S.; Chiappini, C.; Church, R. P.; Csizmadia, Sz.; Cunha, M.; Damasso, M.; Davies, M. B.; Deeg, H. J.; Díaz, R. F.; Dreizler, S.; Dreyer, C.; Eggenberger, P.; Ehrenreich, D.; Eigmüller, P.; Erikson, A.; Farmer, R.; Feltzing, S.; de Oliveira Fialho, F.; Figueira, P.; Forveille, T.; Fridlund, M.; García, R. A.; Giommi, P.; Giuffrida, G.; Godolt, M.; Gomes da Silva, J.; Granzer, T.; Grenfell, J. L.; Grotsch-Noels, A.; Günther, E.; Haswell, C. A.; Hatzes, A. P.; Hébrard, G.; Hekker, S.; Helled, R.; Heng, K.; Jenkins, J. M.; Johansen, A.; Khodachenko, M. L.; Kislyakova, K. G.; Kley, W.; Kolb, U.; Krivova, N.; Kupka, F.; Lammer, H.; Lanza, A. F.; Lebreton, Y.; Magrin, D.; Marcos-Arenal, P.; Marrese, P. M.; Marques, J. P.; Martins, J.; Mathis, S.; Mathur, S.; Messina, S.; Miglio, A.; Montalban, J.; Montalto, M.; Monteiro, M. J. P. F. G.; Moradi, H.; Moravveji, E.; Mordasini, C.; Morel, T.; Mortier, A.; Nascimbeni, V.; Nelson, R. P.; Nielsen, M. B.; Noack, L.; Norton, A. J.; Ofir, A.; Oshagh, M.; Ouazzani, R.-M.; Pápics, P.; Parro, V. C.; Petit, P.; Plez, B.; Poretti, E.; Quirrenbach, A.; Ragazzoni, R.; Raimondo, G.; Rainer, M.; Reese, D. R.; Redmer, R.; Reffert, S.; Rojas-Ayala, B.; Roxburgh, I. W.; Salmon, S.; Santerne, A.; Schneider, J.; Schou, J.; Schuh, S.; Schunker, H.; Silva-Valio, A.; Silvotti, R.; Skillen, I.; Snellen, I.; Sohl, F.; Sousa, S. G.; Sozzetti, A.; Stello, D.; Strassmeier, K. G.; Švanda, M.; Szabó, Gy. M.; Tkachenko, A.; Valencia, D.; Van Grootel, V.; Vauclair, S. D.; Ventura, P.; Wagner, F. W.; Walton, N. A.; Weingrill, J.; Werner, S. C.; Wheatley, P. J.; Zwintz, K., "The PLATO 2.0 mission," Experimental Astronomy, Volume 38, Issue 1-2, pp. 249-330, (2014).

[2] Roberto Ragazzoni; Heike Rauer; Claude Catala; Demetrio Magrin; Daniele Piazza; Isabella Pagano; Valerio Nascimbeni; Giampaolo Piotto; Pierre Bodin; Patrick Levacher; Jacopo Farinato; Valentina Viotto; Maria Bergomi; Marco Dima; Luca Marafatto; Matteo Munari; Mauro Ghigo; Stefano Basso; Francesco Borsa; Daniele Spiga; Gisbert Peter; Ana Heras; Philippe Gondoin; "A one meter class eye for the PLAnetary Transit and Oscillation spacecraft, " Acta Astronautica, Volume 115, pp 18-23, (2015).

[3] Roberto Ragazzoni et al., "PLATO: a multiple telescope spacecraft for exo-planets hunting," Proc.SPIE 9904, (2016)

[4] Magrin, Demetrio; Munari, Matteo; Pagano, Isabella; Piazza, Daniele; Ragazzoni, Roberto; Arcidiacono, Carmelo; Basso, Stefano; Dima, Marco; Farinato, Jacopo; Gambicorti, Lisa; Gentile, Giorgia; Ghigo, Mauro; Pace, Emanuele; Piotto, Giampaolo; Scuderi, Salvatore; Viotto, Valentina; Zima, Wolfgang; Catala, Claude, "PLATO: detailed design of the telescope optical units, " Proc. SPIE 7731, (2010).